Available online at www.sciencedirect.com
SCIENCE DIRECT
Polymer 46 (2005) 11881–11888
polymer
www.elsevier.com/locate/polymer

Molecular dynamics simulation of liquid crystal formation within semi-flexible main chain LCPs

Kai Leung Yung [a], Lan He [a,b], Yan Xu [a,*], Yun Wen Shen [b]

[a] *Department of Industrial Systems and Engineering, The Hong Kong Polytechnic University, Hung Hom, Kowloon, Hong Kong, China*
[b] *Northwestern Polytechnical University, MailBox 278, Xi'An 710072, China*

Received 5 August 2005; received in revised form 29 September 2005; accepted 29 September 2005
Available online 20 October 2005

Abstract

Molecular dynamics simulations of a semi-flexible main chain LCP (liquid crystalline polymer) have been carried out using a newly developed model named solo-LJ-spring-GB model. The new model represents the molecular chain in the form of GB-spring-LJ-spring-…-LJ-spring-GB sections that simplifies the model and reduces the simulation computation by many times. The new model was evaluated by studying the phase behaviors of semi-flexible main chain LCPs through simulation. The results, such as the spontaneous phase transition from isotropic phase to nematic phase as the system temperature decreases and the odd–even effect of the number of flexible spacers on its thermodynamic properties agree well with other experimental results as well as simulations using the traditional GB/LJ model. The orientational and translational mobilities of mesogenic units in the new model have also been measured and compared with those in the traditional GB/LJ model with very little differences found.

Keywords: Liquid crystalline polymers; Solo-LJ-spring-GB model; Molecular dynamics simulation

1. Introduction

LCPs are a new class of macromolecular materials that have great potential in developing micro devices and nano components due to their high stiffness in solid state, low viscosity in the liquid crystalline state and excellent dimensional stability during phase transition [1–4]. These superior properties may be traced to the unique mesophase features of LCPs [4,5]. Hence, recently there are many experimental studies [6–11] on the phase transitions, structures of mesophases and molecular motions during the phase transitions of LCPs. To provide more detailed analysis and explanations to the phase behaviors and dynamic anisotropies that cannot be shown by experiments, simulations such as those for studying the structural and dynamic properties of liquid crystal phases at microscopic scales [12–21] are used.

Up to now, most simulation studies on the liquid crystal materials using MD (molecular dynamics) or MC (Monte Carlo) simulations were on materials with lower molecular weight and simpler molecular structures [16–21] than LCPs. The simple reason is the much larger number of particles in the traditional model of a macromolecule makes the computational complexity unbearably high with unreasonably long computation time. Darinsky et al. [22,23] studied the conformational properties and orientational mobilities of LCPs by the BD (Brownian dynamics) method based on the rigid dumbbell model in viscous medium under the influence of a nematic field. Lyulin et al. [24] studied the effect of varying the spacer length on thermodynamic properties and examined the region of the isotropic–liquid crystalline transition using the GB/LJ model (here called traditional GB/LJ model), in which mesogenic units (GB units) are connected to each other through several flexible methylene spacers (LJ units). Darinskii et al. [25] developed a model consisting of tangent soft spheres connected by elastic springs and investigated the flexibilities and dynamic anisotropies of semi-flexible LCPs using the model. Pavel et al.[26] analyzed the conformation of azobenzene LCPs using an atomistic level model. Atomistic models, although accurate, are extremely expensive computation wise for simulating LCPs. Hence it is very difficult to study together large number of molecular chains to find out their collective phenomena accurately. Therefore, the atomistic models of LCPs are usually used for studying the conformation

* Corresponding author. Tel.: +852 27666572; fax: +852 23625267.
E-mail address: mfxuyan@polyu.edu.hk (Y. Xu).

0032-3861/$ - see front matter © 2005 Elsevier Ltd. All rights reserved.
doi:10.1016/j.polymer.2005.09.081

Nomenclature

w_1	mass compensation coefficient
w_2	strength compensation coefficient
n_s	flexible spacer length
$\hat{\mathbf{u}}_i$, $\hat{\mathbf{u}}_j$	unit vectors along the GB molecular long axes
$\hat{\mathbf{r}}_{ij}$	the separation unit vector between particle i and j
σ^{GB}	the distance function
ε'^{GB}, ε''^{GB}	the orientation dependent well depths
μ, ν	exponential parameters
σ_0	initial distance parameter
ε_0	intial well depth parameter
V_{GB}	potential between a pair of GB particle
$V_{LJ/GB}$	potential between LJ and GB particles
V_{LJ}	potential between LJ particles
V_{sp}	nonlinear spring potential
r_{si}	the distance from the center of the LJ site to the adjacent ending point of the GB site
α_i	the angle between the long axis of the GB site and the separation from the center of the GB site to the center of the LJ site
α_{ijk}	the angle between two displacements from the LJ site to two adjacent GB sites
K_s, K_a, K_t	energy parameters
α_0	the equilibrium angle
r_{s0}	the equilibrium distance
f_s	the energy coefficient in the spring potential
S_2	the orientational order parameter
θ	the angle between the long axis of the GB ellipsoid and the average orientation of the sample
$\mathbf{n}$	the average director
λ_+	the largest eigenvalue
δ	delta function
$Q_{\psi\phi}$	the diagonalization of the ordering tensor
N_{GB}	the number of GB particles
$g(r)$	the radial distribution function
$g_2(r)$	the second-rank orientational distribution function
$P_2(\cos\gamma)$	the second-rank Legendre polynomial
$P_\perp^{(1)}(t)$, $P_\parallel^{(1)}(t)$	the perpendicular and parallel components of orientational autocorrelation function along the director $\mathbf{n}$
$D(t)$	diffusion coefficient function
$D_\parallel(t)$, $D_\perp(t)$	parallel and perpendicular components of $D(t)$

of a single chain. On the other hand, other oversimplified models fail to describe detailed molecular features of semiflexible main chain LCPs, for example, dumbbell and bead-spring models cannot demonstrate the odd–even effect, which curtail the accuracy of simulation. The traditional GB/LJ model has been developed after Gay et al. [27] revised the GB potential for modeling the interactions between mesogenic units in liquid crystal molecules and Cleaver et al. [28] derived the general potential form for computing the interactions between dissimilar uniaxial or biaxial particles. The traditional GB/LJ model has proven to be particularly effective in modeling liquid crystal macromolecules and to be much more efficient than the atomistic level MD models [29–32]. However, the simulation computing time of simulation using the traditional GB/LJ model is still very long. It is found that by modifying the traditional GB/LJ model to a solo LJ/GB model, the efficiency of computation can drastically be improved to 10 times that of the traditional model, allowing larger number of molecular chains being simulated and more collective phenomena being observed. Using this new model called the solo-LJ-spring-GB model, the phase behaviors and local mobilities of a kind of semi-flexible main chain TLCPs (thermotropic liquid crystalline polymers) will be studied. The results are to be compared with the experimental data and simulation using the traditional GB/LJ model.

2. Computational model

The new model is used to roughly mimic a simple main chain TLCP called LC main chain polyester PE1/n, of which the monomer unit is

$$[\text{–COO–C}_6\text{H}_4\text{–COO–C}_6\text{H}_4\text{–COO–C}_6\text{H}_4\text{–COO–(CH}_2)_n\text{–}]_m \quad (1)$$

where, typically $5 \leq n \leq 10$. The material has been synthesized successfully in the early 1980s [33] with series of experimental data showing the odd–even effects of the number of flexible methylene spacers on its thermodynamic properties [34–36]. Here, mesogenic elements in the TLCP are represented by GB units same as that in the traditional GB/LJ model. The flexible spacers between rigid units are modeled by a single (or solo) LJ unit with springs connecting to adjacent GB units (Fig. 1(b)). Usually, the number of flexible spacers (or flexible spacer length) is much larger than the number of rigid units in the traditional model. Hence, by replacing several LJ atoms with a solo LJ unit and two springs, the computation speed can be greatly increased. In the new model, the united LJ site replaces a series of LJ atoms in the traditional model (as shown in Fig. 1(a)) with a mass compensation coefficient w_1

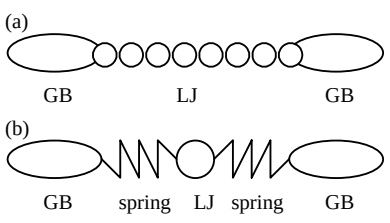

Fig. 1. Schematic diagrams of the new molecular model and the traditional GB/LJ model in a main chain liquid crystalline polymer. (a) The schematic diagram of a unit of a chain in the traditional GB/LJ model. (b) The schematic diagram of a unit of a chain in the new model.

and a strength compensation coefficient w_2. These two coefficients, which are introduced into the interactions between LJ particles themselves as well as between GB particles and LJ particles, are related to flexible spacer length (n_s) in the traditional model by the following equations:

$$w_1 = \frac{(n_s^3 - n_s - 0.5)}{n_s^2}, \qquad w_2 = \frac{4(n_s - 3)}{n_s} \tag{2}$$

The interaction energy between a pair of mesogenic elements is given by the GB potential [27]

$$V_{GB} = 4\varepsilon_0^{GB}[\varepsilon''^{GB}(\hat{\mathbf{u}}_i, \hat{\mathbf{u}}_j)]^{\nu}[\varepsilon'^{GB}(\hat{\mathbf{u}}_i, \hat{\mathbf{u}}_j, \hat{\mathbf{r}}_{ij})]^{\mu} \times \left[\left(\frac{\sigma_0^{GB}}{r_{ij} - \sigma^{GB}(\hat{\mathbf{u}}_i, \hat{\mathbf{u}}_j, \hat{\mathbf{r}}_{ij}) + \sigma_0^{GB}}\right)^{12} - \left(\frac{\sigma_0^{GB}}{r_{ij} - \sigma^{GB}(\hat{\mathbf{u}}_i, \hat{\mathbf{u}}_j, \hat{\mathbf{r}}_{ij}) + \sigma_0^{GB}}\right)^{6}\right] \tag{3}$$

where, $\hat{\mathbf{u}}_i$ and $\hat{\mathbf{u}}_j$ are unit vectors along the GB molecular long axes, $\hat{\mathbf{r}}_{ij} = \mathbf{r}_{ij}/\mathbf{r}_{ij}$ is the separation unit vector between particle i and j. σ^{GB} is the distance function which depends on the relative orientations of the elements and the unit vectors $\hat{\mathbf{r}}_{ij}$. ε'^{GB} and ε''^{GB} are the orientation dependent well depths. σ^{GB}, $[\varepsilon'^{GB}]^{\mu}$ and $[\varepsilon''^{GB}]^{\nu}$ are given by Eqs. (2) and (3) of Ref. [37]. Here, the length to breadth ratio is set as $\sigma_{ee}/\sigma_{ss} = 3$, the ratio of well-depth for end-to-end and side-to-side particles is set as $\varepsilon_{ee}/\varepsilon_{ss} = 1/5$ and the parameters $\mu = 2$, $\nu = 1$, being the same as those in the traditional model simulation [24]. Meanwhile, the values of $\sigma_0^{GB} = 0.4721$ nm and $\varepsilon_0^{GB} = 6.76$ KJ/mol are used in our simulation. From the work of Cleaver et al. [28] the interaction energy between a GB particle and a LJ unit is defined as the generalized potential:

$$V_{LJ/GB} = 4w_2\varepsilon^{LJ/GB}(\hat{\mathbf{u}}_j, \hat{\mathbf{r}}_{ij})\left[\left(\frac{\sigma_0^{LJ/GB}}{r_{ij} - \sigma^{LJ/GB}(\hat{\mathbf{u}}_j, \hat{\mathbf{r}}_{ij}) + \sigma_0^{LJ/GB}}\right)^{12} - \left(\frac{\sigma_0^{LJ/GB}}{r_{ij} - \sigma^{LJ/GB}(\hat{\mathbf{u}}_j, \hat{\mathbf{r}}_{ij}) + \sigma_0^{LJ/GB}}\right)^{6}\right] \tag{4}$$

where, $\sigma^{LJ/GB}$ and $\varepsilon^{LJ/GB}$ are given, respectively, by Eqs. (20) and (37) of Ref. [28]. Values of $\sigma_0^{LJ/GB} = 0.4117$ nm and $\varepsilon_0^{LJ/GB} = 1.42$ KJ/mol are used in the same way as Ref. [24]. The interaction energy between two united LJ particles is given by the standard shifted 12:6 LJ potential [38]:

$$V_{LJ} = w_2\left\{4\varepsilon_0^{LJ}\left[\left(\frac{\sigma_0^{LJ}}{r_{ij}}\right)^{12} - \left(\frac{\sigma_0^{LJ}}{r_{ij}}\right)^{6}\right] + \varepsilon_0^{LJ}\right\}, \tag{5}$$

$$r_{ij} \Leftarrow r_c,\ r_c = 2^{1/6}\sigma_0^{LJ}$$

where, σ_0^{LJ} and ε_0^{LJ} equal 0.3923 nm and 0.6 KJ/mol, respectively as in Ref. [24]. The nonlinear spring potential takes the following form:

$$V_{sp} = -0.5K_s(r_{si} - r_{s0})^2 + 0.5K_a f_s(\alpha_i - \alpha_0)^2 + 0.5K_t(\alpha_{ijk} - \alpha_0)^2 \tag{6}$$

where r_{si} is the distance from the center of the LJ site to the adjacent ending point of the GB site, α_i is the angle between the long axis of the GB site and the separation from the center of the GB site to the center of the LJ site and α_{ijk} is the angle between two displacements from the LJ site to two adjacent GB sites. The energy parameters K_s, K_a, K_t assumed values of 3.6129×10^{-20}, 8.654×10^{-19}, 8.654×10^{-19} J, respectively in this work. The equilibrium angle is defined as $\alpha_0 = 180°$. The equilibrium distance is given by

$$r_{s0} = \frac{0.5(3n_s - 5.0)}{2.0} \tag{7}$$

This equation is used to change the corresponding length of a molecular chain with different number of flexible spacers in this model. The energy coefficient f_s is related to the number of flexible spacers by the equation:

$$f_s = \frac{2(f_I + 1.0)}{n_s} \tag{8}$$

where, f_I is equal to the integer value of $n_s/2.0$.

3. Method of simulation

To compare the solo-LJ-spring-GB model with the traditional GB/LJ model, the scale of the simulation system, the ensembles and the initial conditions are taken to be the same as those in Ref. [24]. The simulation system includes 64 polymer chains with the degree of polymerization (the number of GB units) $M = 10$. The initial configuration is started from a low molecular density in an all-trans configuration aligned parallel to the z-axis of the simulation box. Molecules are arranged with a random center of mass vector and particle velocities are taken from a Maxwell–Bolzmann distribution. A standard leap-frog algorithm for anisotropic systems [39] is used to solve the equations of motions. The time step is 2fs. Initial calculation employs the NPT ensemble, using extended system method [40] to generate the system equilibration. Constant pressure P is equal to zero and constant temperature varies from 500 to 350 K in the NPT ensemble. In all cases equilibration takes 6–9 ns. After equilibration, the NVE ensemble is performed to collect results at selected equilibrated state points. The duration of production run varies from 600 to 800 ps on a workstation with 16×1.2 GHz ultra SunSparc CPUs. During the production run, the orientational and translational orderings of the GB sites are monitored. The former is defined through the calculation of the orientational order parameter,

$$S_2 = \langle P_2(\cos\theta)\rangle = \langle 3/2\cos^2\theta - 1/2\rangle \tag{9}$$

where, θ is the angle between the long axis of the GB ellipsoid and the average orientation of the sample, which is defined by the director **n**. In this simulation, S_2 is associated with the largest eigenvalue λ_+ obtained through the diagonalization of

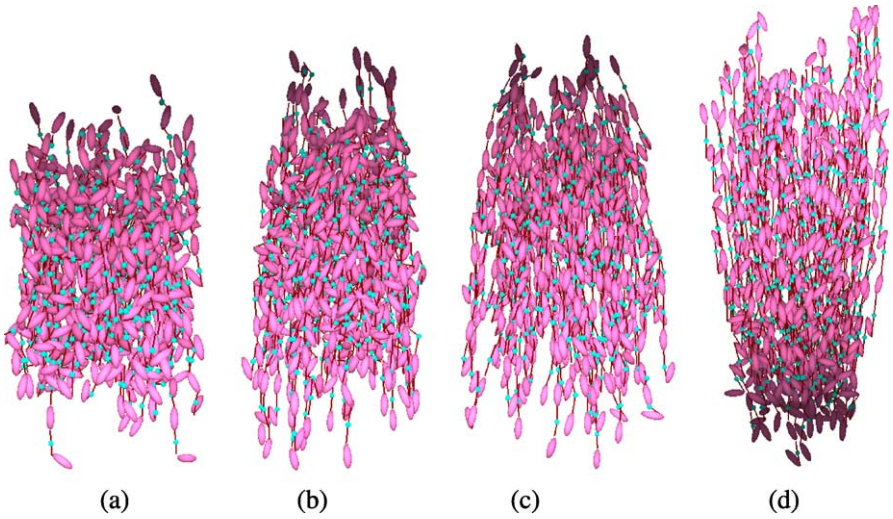

Fig. 2. Snapshots of a polymer system with $n_s=6$ (a) The configuration at $T=500$ K. (b) The configuration at $T=400$ K. (c) The configuration at $T=370$ K. (d) The configuration at $T=350$ K.

the ordering tensor,

$$Q_{\psi\phi} = \frac{1}{N_{GB}} \sum_{i=1}^{N_{GB}} \frac{3}{2} \mathbf{u}_{i\psi} \mathbf{u}_{i\phi} - \frac{1}{2} \delta_{\psi\phi}, \quad \psi, \phi = x, y, z \tag{10}$$

The eigenvector associated with λ_+ provides the director $\mathbf{n}$ for describing the average direction of alignment for GB particles. The latter is described through the radial distribution function (Eq. (10)) for pairs of GB sites that provides insight into the liquid crystalline polymer structure

$$g(r) = \frac{V}{[N_{GB}]^2} \left\langle \sum_{i}^{N_{GB}} \sum_{j \neq i}^{N_{GB}} \delta(\mathbf{r} - \mathbf{r}_{ij}) \right\rangle \tag{11}$$

4. Simulation results and discussions

4.1. Phase transition phenomena

The liquid crystalline polymer melt shows the phase transition phenomenon as the system temperature drops from 500 to 350 K. Fig. 2 presents the snapshots of a TLCP system with the flexible spacers $n_s=6$, where phase transition from isotropic to liquid crystalline takes place step by step. It shows that at the system temperature $T=400$ K and $T=500$ K (Fig. 2(a) and (b)), the polymer chains entangle each other and have no alignment order exhibiting typical isotropic phase. Decreasing the system temperature to 350 K leads to the spontaneous orientational ordering (Fig. 2(d)). The visualization of the arrangement of molecular chains (Fig. 2(d)) suggests the liquid crystalline phase presented here is nematic, which will be further confirmed in the distribution function analyses.

The structure of molecules in polymer melt can be characterized by a series of distribution functions. In our simulation, the radial pair distribution function (Eq. (11)) and the second-rank orientational distribution function are employed to investigate the phase transition of a TLCP melt. The second-rank orientational distribution function takes the form:

$$g_2(r) = \langle P_2(\cos \gamma_{ij}(r)) \rangle \tag{12}$$

where $P_2(\cos\gamma)$ is the second-rank Legendre polynomial and $\gamma_{ij}(r)$ denotes the angle between the long axes of a pair of GB particles (i and j) situating in a narrow shell of center-of-mass separations $r_{ij} \approx r$.

The radial pair distribution and second-rank orientational distribution functions for GB sites in the polymer (with the spacer length $n_s=6$) are measured and shown in Figs. 3 and 4. Fig. 3 shows there are very few peaks in $g(r)$ (where fluctuant values near 0.1) at higher temperatures $T=500$ K and $T=400$ K, which indicates positional correlation between neighboring sites is weak. The corresponding values of $g_2(r)$ (Fig. 4) at these temperatures decay smoothly very close to zero from $r/\sigma \approx 2.0$ to sufficiently large distances. These curves confirm that the configuration in Fig. 2(a) and (b) forms an isotropic phase, which accords with the values of the orientational order

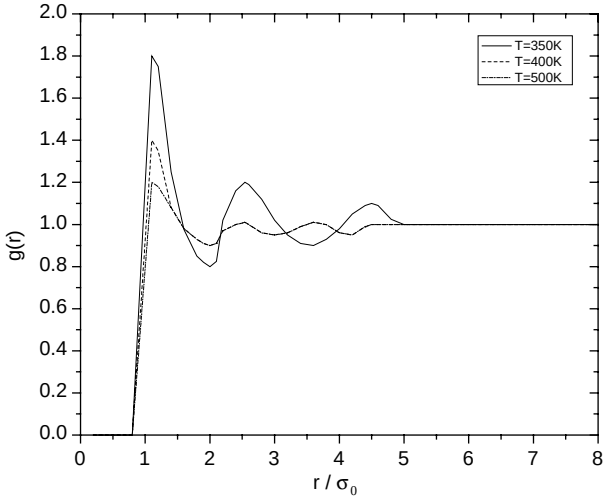

Fig. 3. Pair distribution function. $T=350$ K (solid line), 400 K (dashed line), 500 K (dot-dash line). The curves for $T=370$ K are very similar to $T=350$ K.

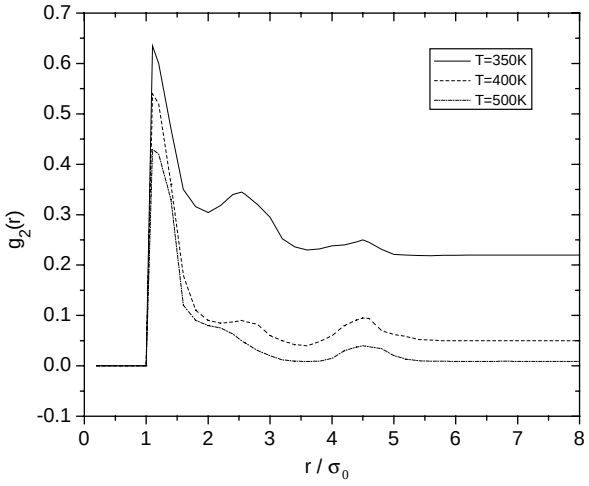

Fig. 4. Orientational distribution function $g_2(r)$. $T=350$ K (solid line), 400 K (dashed line), 500 K (dot-dash line). The curves for $T=370$ K are very similar to $T=350$ K.

parameters $S_2=0.13$ and $S_2=0.29$, respectively, at $T=500$ K and $T=400$ K (in the polymer with the spacer length $n_s=6$) shown in Fig. 5.

The function $g(r)$ at the system temperature $T=350$ K (Fig. 3), unlike that of low molecular weight system in the smectic phase that displays strong oscillations in the wide range of the separation [29], firstly shows two peaks and troughs and then tends to the constant value of 1.0 at large separation, which implies the liquid crystalline phase presented here is nematic. The fact that the liquid crystalline phase at lower temperature shown in this model is nematic can be proven further by analyzing the function $g_2(r)$ (Fig. 4). The values of the function $g_2(r)$ at larger separations (r) in the liquid crystalline phase approach the constant value of 0.22 that equals approximately to the square of the relative orientational order parameter $S_2\approx0.49$ (as shown in Fig. 5). This agrees well with Refs. [24,29]. Moreover, the function $g_2(r)$ shows two peaks at smaller r (as shown in Fig. 4). The principal peak at

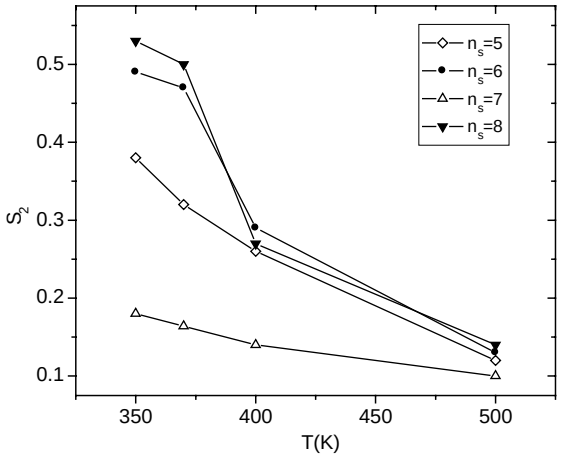

Fig. 5. Orientational order parameter as a function of the temperature. $n_s=5$ (diamonds), $n_s=6$ (circles), $n_s=7$ (up triangles), $n_s=8$ (down triangles) odd–even effect are highlighted by using filled symbols for even n_s and open symbols for odd n_s.

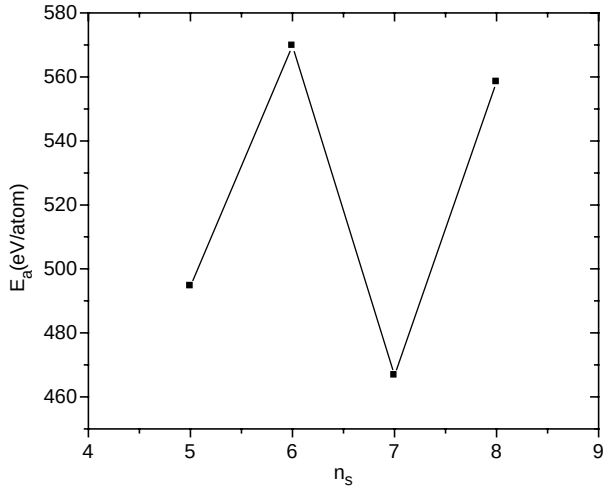

Fig. 6. Plots of average equilibrium energy of the polymer chain in the new model versus the spacer length at the system temperature $T=350$ K.

$r/\sigma_0\approx2.5$ reflects some short-range side-by-side ordering and the small peak at $r/\sigma_0\approx4.5$ indicates strong orientational correlation between GB particles within the liquid crystalline molecules. In Ref. [24] these two peaks lie in $r/\sigma_0\approx2.0$ and $r/\sigma_0\approx4.0$, respectively. The peaks presented in our simulation are shifted by 0.5 forward when compared to those in Ref. [24]. A possible reason is that the system density presented here (0.71 shown in Fig. 6), at $T=350$ K, is a bit lower than that (0.76) shown in Ref. [24], which suggests that this model is slightly more flexible than the traditional model.

4.2. Odd–even effect

The distribution functions and the orientational order parameter are also measured for GB particles in the polymer with $n_s=5$, 7, 8. Fig. 5 presents the values of orientational order parameter for GB particles at different equilibrium temperatures. For the systems with $n_s=7$ and $n_s=5$, the values of orientational order parameter do not vary as much as those for $n_s=8$ and $n_s=7$ when the system temperature is reduced from $T=500$ K to $T=350$ K (Fig. 5). It is obvious that S_2 is higher for polymers with the spacer length n_s being even than that with n_s being odd at the same temperature. This odd–even effect agrees with the experimental observations [41] and the simulation results in Ref. [24]. By comparing Fig. 5 with Fig. 5 of Ref. [24], the current model shows a slightly stronger tendency to produce orientational ordering state than the traditional model.

The odd–even effect of the orientational order parameter, which depends on the flexible spacer length, can be explained in detail through the odd–even fluctuation of the equilibrium energy (or activation energy) as shown in Fig. 6. The activation energy of a polymer chain (E_a) is higher for polymers with even spacer length than those polymers with odd spacer length, agrees with the experimental results [42]. It implies that molecular chains in polymers with flexible spacer length n_s being odd have stronger tendency to form self-conformation (where molecular chains prefer to entangle so that the system

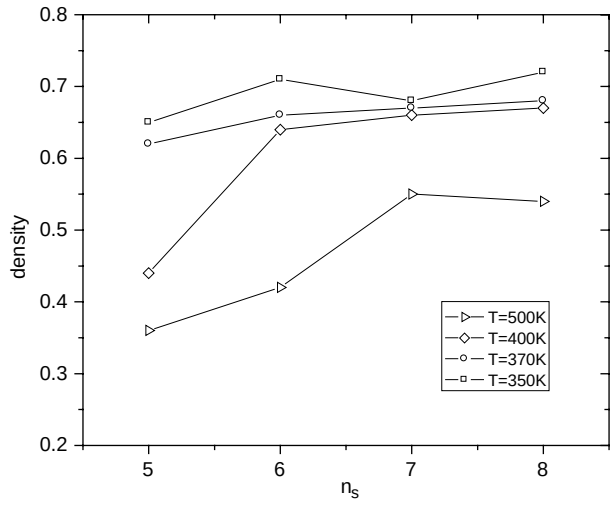

Fig. 7. Equilibrium density as a function of the spacer length at temperatures $T=350$ K (squares), $T=370$ K (circles), $T=400$ K (diamond), $T=500$ K (right triangles).

energy gets to the minimum) than those with flexible spacer length n_s being even. Hence, the orientational order parameter values of the polymers with odd number of flexible spacers are lower than those of the polymers with even number of flexible spacers.

The odd–even effect can also be observed at the equilibrium density in the liquid crystalline state (Fig. 7). The equilibrium density at given T and $P=0$ is higher for even n_s, and lower for odd n_s, which agrees with the experimental observations [43] and the results in Ref. [24].

4.3. Local mobility

To compare the new model with the traditional model in detail, the orientational and translational mobility are investigated. The orientational autocorrelation function $P^{(1)}(t)$ resolved into two components $P^{(1)}_{\perp}(t)$ and $P^{(1)}_{||}(t)$ along the director **n** is used to study the orientational mobility of GB particles. The functions $P^{(1)}_{\perp}(t)$ and $P^{(1)}_{||}(t)$ are defined in Eqs. (13) and (14).

$$P^{(1)}_{\perp}(t) = \frac{\langle \cos\varphi(0)\cos\varphi(t)\rangle}{\langle \cos^2\varphi\rangle} \tag{13}$$

$$P^{(1)}_{||}(t) = \frac{\langle \cos\beta(0)\cos\beta(t)\rangle}{\langle \cos^2\beta\rangle} \tag{14}$$

Here β and ϕ are the angles made by the long axis of the GB particle with the director **n** and with a perpendicular direction, respectively. The orientational correlation functions for GB particles of the polymer system with $n_s=6$ in the isotropic phase and the nematic phase are calculated and their results being shown in Fig. 8. Comparing with Fig. 10 in Ref. [24], mesogenic elements in the current model perform analogous formation of orientational motion as in the traditional model. In isotropic phase, the functions decay quickly to small values in short relaxation time. In nematic phase, the relationship

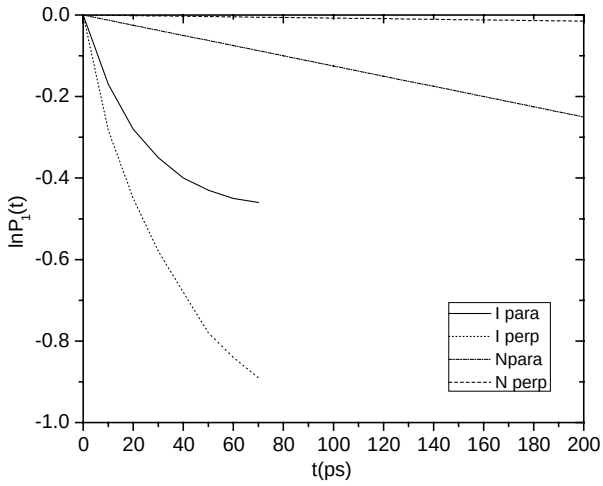

Fig. 8. Orientational parallel and perpendicular correlation function for Gay–Berne elements in polymer chains.

between the functions and relaxation time is linear and the parallel orientational motion changes much slower than the perpendicular motion as relaxation time increases.

To study local translational mobility of mesogenic elements at different system temperatures, diffusion coefficient function $D(t)$, which is resolved into parallel and perpendicular components $D_{||}(t)$ and $D_{\perp}(t)$ to the director **n**, is calculated. Here $D(t)$ is given as:

$$D(t) = \frac{\langle |\mathbf{r}_i(t) - \mathbf{r}_i(0)|^2\rangle}{6t} \tag{15}$$

The temperature dependent translational diffusion functions for GB particles in polymers with $n_s=5$ and $n_s=6$ are shown in Fig. 9. It shows that the parallel diffusion coefficient is larger than the perpendicular diffusion coefficient at the same system temperatures. This agrees with the common knowledge that LCPs exhibit a dynamical anisotropy that the self-diffusion of molecules along the director **n** is easier than that in normal

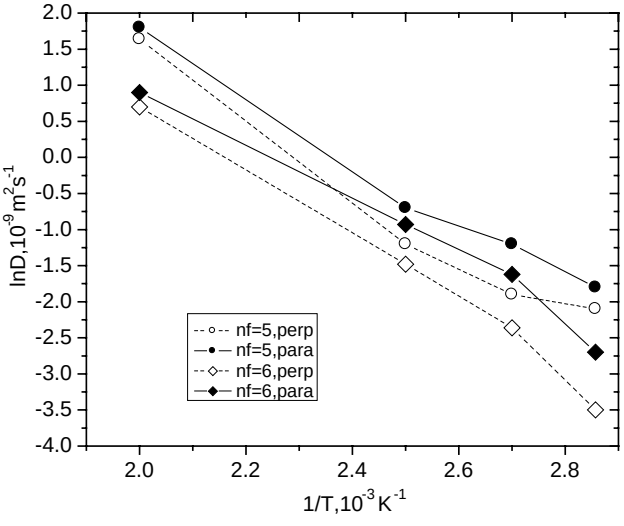

Fig. 9. Parallel (filled symbols) and perpendicular (open symbols) translational diffusion functions versus the system temperature for polymer systems with $n_s=5$ and $n_s=6$.

Table 1
The comparison of computational cost between the hybrid model and current model

N_c	$N1$[a]	$N2$[a]	$T1$ (s)	$T2$ (s)
36	2304	684	28	5
64	4096	1216	82	12
100	6400	1900	177	24
144	9216	2736	340	41
169	10,816	3211	453	45

Benchmark figures on a IBM T42 PM 1.6 GHz. N_c, the number of chains; $N1$, the total number of particles calculated in hybrid GB/LJ model; $N2$, the total number of particles calculatedin the current model; $T1$, the CPU running time of simulating 50 steps for hybrid GB/LJ model; $T2$, the CPU running time of simulating 50 steps for the current model.

[a] Polymerization $M=10$, flexible spacers $m=6$, $n_s=6$.

direction. Also shown in Fig. 9 is both the parallel and perpendicular diffusion coefficients decrease as the system temperature reduces. Meanwhile the parallel and perpendicular diffusion coefficients also decrease as the order parameter S_2 increases when GB particles are in nematic phase (in Fig. 9: $\ln D$ for $n_s=5$ and $n_s=6$ at $T=350$ K). These phenomena suggest that mesogenic elements have weak translational mobility in liquid crystalline phase.

4.4. The computational efficiency

The respective computing costs of the new model and the traditional model during MD simulation of semiflexible main chain TLCPs with flexible spacer length $n_s=6$ are shown in Table 1. It shows that the computing efficiency of the current model is much higher than that of the traditional model. The CPU time required for the current model occupies only about 18% of that required for the traditional model when the total number of molecular chains is 40. It costs less than 10% run time of the traditional model when the number of molecular chains exceeds 150 indicating that the larger the number of chains the better the new model is. Hence, the new model provides a more efficient way for studying structural properties and dynamic behaviors of semi-flexible main chain LCPs at large-scale.

5. Conclusions

This paper has presented a more efficient new molecular model for simulating semiflexible main-chain liquid crystalline polymers. The model has been compared with the traditional GB/LJ model through studying phase behaviors and mobility with respect to orientation and translation for a main-chain PE1 with various spacer length n_s. It is found that the two models give analogous results. By examining the orientational order parameter S_2, the radial pair distribution function $g(r)$, the second-rank orientational distribution function $g_2(r)$ and visualization of configuration snapshots, the isotropic and nematic phases are identified. The odd–even effects are also observed in the orientational order parameter S_2, the activation energy E_a and the equilibrium density ρ. Intensive comparisons have shown that the new model exhibits similar molecular behaviors as the traditional model with slightly better elongating ability and translational mobility.

The results show that the protocol of this model requires less than 10% of the computer time when compared with the traditional GB/LJ model (given the number of flexible spacer is 6 and the total number of molecular chains is 150). This allows for simulating molecular behaviors of LCPs in longer time periods at larger system. The new model not only can be employed to study the structural properties and phase behaviors of LCPs but also has great potential in exploring the flow behaviors and interface problems of main chain semiflexible liquid crystalline polymers such as those in the injection molding process of TLCPs for fabricating micro devices.

We regard the results of the present work as an encouraging sign for future simulation study of LCPs confined in a nano channel in the near future.

Acknowledgements

The work described in this paper was supported by the Hong Kong Polytechnic University Central Research Grant (G-T676)
.

References

[1] Wang YL, Yue CY, Tam KC, Hu X. J Appl Polym Sci 2003;88:1713.
[2] Lekakou C. Polym Eng Sci 1997;37:529.
[3] Mori N, Tsuji Y, Nakamura K, Yoshikawa C. J Non-Newtonian Fluid Mech 1995;56:85.
[4] Donald AM, Windle AH. Liquid crystalline polymer. Cambridge, UK: Cambridge University Press; 1992 p. 235.
[5] Wang X-J, Zhou Q-F. Liquid crystalline polymer. Singapore: World Scientific; 2004 p. 245.
[6] Blumstein A, Thomas O. Macromolecules 1982;15:1264.
[7] Chang S, Han CD. Macromolecules 1997;30:1670.
[8] Han CD, Chang S, Mather PT, Fang X. Macromolecules 2001;34:7152.
[9] De Abajo J, De la Campa JG, Kricheldorf HR, Schwarz G. Makromol Chem 1990;191:537.
[10] Watanabe J, Hayashi M. Macromolecules 1988;21:278.
[11] Strzelecki L, Van Luyen D. Polym J 1980;16:299.
[12] Bionski S, Brostow W. J Chem Phys 1991;95:2890.
[13] Allen MP, Warren MA, Wilson MR. Phys Rev E 1998;57:5585.
[14] Melker AI, Efleev AN. J Macromol Sci Phys 1999;B38:769.
[15] Kremer K. J Chem Phys 1990;92:5057.
[16] Patnaik SS, Lupo JA, Pachter R. Comput Theor Polym Sci 1998;8:39.
[17] de Miguel E, de Rio EM. J Chem Phys 1996;105:4234.
[18] Mcbride C, Wilson MR, Howard JAK. Mol Phys 1998;93:955.
[19] Al-Barwani MS, Allen MP. Phys Rev E 2000;62:6706.
[20] Perera A, Ravichandran S, Moreau M. J Chem Phys 1997;106:1280.
[21] Wang Z, Lupo JA, Patnaik S, Pachter R. Comput Theor Polym Sci 2001; 11:375.
[22] Darinskii A, Lyulin A, Neelov I. Markromol Chem Theory Simul 1993;2:523.
[23] Darinskii A, Gotlib Y, Lukyanov M, Lyulin A, Neelov I. Prog Colloid Polym Sci 1993;91:13.
[24] Lyulin AV, Al-Barwani MS, Allen MP. Macromolecules 1998;31:4626.
[25] Darinskii AA, Neelov IM, Zarembo A, Balabaev NK. Macromol Symp 2003;191:191.
[26] Pavel D, Shanks R, Sangari S, Alazaroaie S, Hurduc N. Macromol Theory Simul 2003;12:127.
[27] Gay JG, Berne BJ. J Chem Phys 1981;74:3316.
[28] Cleaver DJ, Care CM, Allen MP, Neal MP. Phys Rev E 1996;53:1.

[29] Wilson MR. J Chem Phys 1997;107:20.
[30] Mcbride C, Wilson MR. Mol Phys 1999;97:4.
[31] Zannoni C. J Mater Chem 2001;11:2637.
[32] Perera A, Ravichandran S, Moreau M. J Chem Phys 1997;106:1280.
[33] Bilibin AY, Tenkovtsev AV, Prianer ON, Pashkovsky EE, Skorohodov SS. Makromol Chem 1985;186:1575.
[34] Frosini V, De Petris S, Chielini E, Galli G. Mol Cryst Liq Cryst 1983;93:232.
[35] Ober ChK, Jin JI, Lenz RW. Makromol Chem 1983;4:49.
[36] Shilov VV, Dmitruk NV, Goihman ASh, Skorokhodov SS, Bilibin AY. Vysokomol Soedin Ser B 1987;29:627.
[37] de Miguel E, del Rio EM, Brown JT, Allen MP. J Chem Phys 1996;105:4234.
[38] Earl DJ, Ilnytskyi JM, Wilson MR. Mol Phys 2001;99:1719.
[39] Wilson MR, Allen MP, Warren MA, Sauron A, Smith W. J Comput Chem 1997;18:478.
[40] Iinytskyi JM, Wilson MR. Comput Phys Commun 2002;148:43.
[41] Pardey R, Shen D, Gabori PA, Harris FW, Cheng SZD, Adduci J, et al. Macromolecules 1993;26:3687.
[42] Mizuno M, Hirai A, Matsuzawa H, Endo K, Suhara M, Kenmotsu M, et al. Macromolecules 2002;35:2595.
[43] Krigbaum WR, Watanabe J, Ishikawa T. Macromolecules 1983;16:1271.